MODELING A RADIOGRAPHIC X-RAY IMAGING FACILITY WITH THE PENTRAN PARALLEL S_N CODE

G. E. Sjoden, R. N. Gilchrist, and D. L. Hall
Department of Mathematical Sciences, USAF Academy
USAF Academy, Colorado, USA
joedean@sprintmail.com; rob.gilchrist@usafa.af.mil; deborah.hall@usafa.af.mil

C. A. Nusser, M.D.
Department of Radiology, 10th Medical Group
USAF Academy Hospital, Colorado, USA
chris.nusser@usafa.af.mil

ABSTRACT

This is a paper on the determination of photon fluence and x-ray dose in a radiographic imaging facility at the USAF Academy Hospital, Colorado. The facility, X-ray Room #2, was modeled with the 3-D multi-group discrete ordinates PENTRAN™ parallel transport code system. The 90 cubic meter room was discretized into approximately 131,000 3-D Cartesian cells using a mesh generated by the PENMSH™ code in the PENTRAN system. The BUGLE-96 cross section library was used to generate four-group photon cross sections. The source was an 80kV radiographic tungsten-anode 32 mAs x-ray burst; a spectrum from the literature was adapted to the BUGLE-96 group structure. The source was modeled as a collimated, angular-dependent surface source placed on top of a patient tissue phantom. Group dependent boundary albedos were determined from explicit PENTRAN models of the walls and floor. Results from an S_4 angular quadrature using P_1 anisotropy are presented. In spite of the use of a low order quadrature set, dose estimates from the computational results were in excellent agreement (~1% relative difference) with experimental dose data. Scattering and attenuation of photons, especially severe attenuation of colder x-rays in dense objects, can be readily observed in the data. Overall, it is demonstrated that the PENTRAN code system can be directly applied to model x-ray behavior in this type of facility.

1. INTRODUCTION

With the advent of advanced numerical methods, parallel codes, and parallel computer architectures, deterministic radiation transport calculations can be performed for large problems in a relatively short time. This paper is a summary report of our recent progress in an ongoing effort to model the photon flux (fluence) and estimate the x-ray dose throughout X-ray Room #2 at the USAF Academy Hospital, Colorado. In addition, a broader goal is to demonstrate that the discrete ordinates (S_N) method can be readily used to provide detailed information about the behavior of scattered radiation in x-ray imaging facilities. For this paper, we focus on our PENTRAN™ model of 80kV (32 mAs burst) x-rays, typical of radiographic x-rays routinely used throughout the medical community. A brief discussion of Room #2 geometry and the

computational tools brought to bear on the problem are presented in Section 2. In Section 3, we discuss some of the approximations made to facilitate the calculation, including the formulation of cross sections, discretization of the geomtery, and other pertinent details. This is followed by a presentation of the computational results in Section 4, which include a comparison of the calculated dose to experimental dose for an 80 kV source in Room #2. Subsequent sections provide conclusions, acknowledgements, references, tables, and figures as appropriate.

2. BACKGROUND

2.1 X-RAY ROOM #2

X-ray Room #2 at the USAF Academy Hospital was selected for this model. This is a general-purpose facility used for (short burst) radiographic imaging of fractures, etc. In addition, this same facility is also used for steady-state fluoroscopic imaging in a steady power beam for in-depth, real-time diagnosis. In this paper, only radiographic models are presented. Room #2 is equipped with a tungsten rotating anode x-ray tube for radiographic imaging, and is used up to a maximum potential of 115 kV. Room #2 is large, occupying over 90 cubic meters. It measures 575.95 cm in length (x-axis), 549.91 cm in width (y-axis), and 287.02 cm high (z-axis). The z-axis dimension is based on a measure from the concrete floor up to a thin suspended ceiling in the room; the actual concrete barrier ceiling is much higher, with free space (air) and a network of utility pipes and cables above the suspended ceiling. A 3-D schematic of X-ray Room #2 at USAF Academy Hospital is presented in Figure 1.

2.2 ROOM PRIMARY SHIELDING

Referring to Figure 1, the inside wall at x=158.75 cm, and the outer walls at x=0, x=575.95 cm, y=0, and y=549.91 cm of Room #2 serve as primary shielding, and contain 0.238 cm (3/32 in) of lead, followed by 1.27 cm (0.5 in) of commercial gypsum board with an air gap. Closet doors and a shielded window for operator observation (not shown along the inside wall) contain an equivalent thickness of primary shielding. For purposes of this study, the doors and the window were assumed to be identical to shielded wall materials. The origin was established at (0,0,0) in the lower right corner of Figure 1, and is where a leaded interlocked door to the facility is located. The operator bunker is located to the immediate left (along the y-axis) of the entry. The storage cabinets in the room are stainless steel and glass, while the electronics cabinets contain circuitry housed in carbon steel. Note the Image Intensifier/Electronics Assembly is retractable and is only used for fluoroscopic measurements; since fluoroscopic sources are not presented here, we treat the assembly as retracted against the wall as shown in Figure 1. We further note that the Image Intensifier/Electronics assembly, Rack of Personnel Shields, and the Patient Support/Imaging Table are complex structures that are approximated using parallelepipeds as shown. Overall, this schematic diagram was used as a basis for forming the discretized mesh necessary for the discrete ordinates calculation.

2.3 PENTRAN CODE SYSTEM

Typically, photon flux/fluence determinations in x-ray imaging facilities are obtained via Monte Carlo techniques, or are estimated using limited point-kernel methods and traditional x-ray facility regulatory guidelines. This type of problem indeed poses a particular challenge for discrete ordinates, especially considering the large size of the facility and associated numerical difficulties (potential ray-effects, large regions of nearly-void room air, primary lead and concrete boundary shielding, the need for an angular dependent surface source, and proper component representation). The PENTRAN (Parallel Environment Neutral-particle TRANsport) parallel discrete ordinates code system can be used to overcome most of these difficulties.[1] PENTRAN is a multi-group, anisotropic discrete ordinates code for 3-D Cartesian geometries; it has been specifically designed to solve the linear Boltzmann equation on distributed memory, scalable parallel computer architectures. A variety of domain decomposition alternatives can be specified in PENTRAN by the user for automatic distribution and subsequent iterative solution on a distributed parallel computer that supports message passing via the MPI (Message Passing Interface) library. Specifically, solution of a transport problem can be rendered using automatic domain decomposition among the angular, energy, and spatial variables, including any desired hybrid decompositions among all three domains.

PENTRAN has been extensively tested, and has been shown to accurately compute neutral particle flux solutions for a variety of test problems (compared with traditional codes), and more recently rendered solutions in excellent agreement with experimental data.[2] PENTRAN is supported by a suite of codes that permit one to readily generate 3-D models and gather parallel data. The computational model discussed in this paper was generated using PENMSH™, a mesh generator for 3-D Cartesian geometries. Another code that processes the PENMSH output, called PENINP™, automatically generates a 3-D input deck ready for processing in PENTRAN, including an automated fixed source linear projection of the source distribution. PENMSH renders 2-D *x-y* slices at selected *z*-levels for visual verification of the geometry. Post processing of parallel data stored in multiple files is performed by PENDATA™ to seamlessly gather parallel results for the user, with interpolation using the PENPRL™ or the 3DI™ tool. [3,4]

2.4 PARALLEL COMPUTER PLATFORM

All calculations performed for this paper were accomplished on a parallel SPARKYcluster™ two-processor system using VAST™ Fortran-90 linked with LAM-MPI. This is a distributed parallel computing cluster connected using a fast-ethernet switch; each stand alone machine contains a 380 MHz AMD K6-2 chip with 192 Mb of RAM running Linux 5.2. [5,6,7]

3. DISCRETE ORDINATES MODEL

3.1 MATERIAL TREATMENTS

Room #2 contained many solid objects with a number of constituents. These include stainless steel and glass storage cabinets, steel electronics cabinets, the support/imaging table, a patient

tissue phantom, a storage rack for leaded personnel shield jackets, the lead/drywall shielded operator bunker and surrounding walls, and a drywall-only partition. Due to the number of materials present in the room, and the large computational requirements necessary to model each object in detail, we homogenized bulk materials based on the mass fraction of elements present. In some cases, we made engineering estimates when specific design data were unavailable for each object. In doing so, we carefully measured the dimensions of each object and used densities to preserve mass. All material densities and constituent elements were found in the literature.[8, 9]

3.2 CROSS SECTION TREATMENT

Broad-group photon cross sections were derived and mixed from material mass fractions and bulk densities using the BUGLE-96 library (weighted with a concrete flux spectrum). We made the assumption that these cross sections would be generally applicable to our problem. For this work, we considered photons with energies no higher than 80 keV. Therefore, we generated cross sections using only the last 4 energy groups (64 through 67) of the BUGLE-96 library.[10] Again, all macroscopic cross sections in X-ray Room #2 were determined based on the material composition of homogenized components in the facility.

3.3 PENMSH MODEL ASSEMBLY

X-ray Room #2 at USAFA was modeled using a 3-D Cartesian meshing scheme. The origin of the coordinate system was located in the lower corner of the room to the right of the entrance. The positive *x*-axis was to the right along the wall, and the positive *y*-axis was along the front wall of the room; the positive *z*-axis (upwards) completed a standard right-handed 3-D Cartesian system. There are three kinds of mesh cells that are used by PENTRAN in modeling the room—coarse, medium, and fine mesh cells. Initially, a room is divided into a number of large coarse meshes. The *x*, *y,* and *z* boundaries of the coarse meshes are user defined, and are established around areas of interest.

For this model, the six *x*-coarse mesh boundaries were drawn at 0.0 cm, 111.76 cm, 248.92 cm, 374.0 cm, 439.43 cm, and 575.95 cm. The five *y*-coarse mesh boundaries were drawn at 0.0 cm, 58.42 cm, 149.86 cm, 361.95 cm, and 549.19 cm. Each of the eight *z*-levels in the model contained twenty coarse meshes (an example of *z*-level 3 is given in Figure 2). As in the *x* and *y* dimensions, the *z* boundaries (*z*-levels) were user specified spanning boundaries of particular interest. For example, *z* -level 3 was defined to encompass the patient tissue phantom that is directly subjected to *x*-radiation. For this model the *z*-level boundaries are drawn at 0.0 cm, 60.16 cm, 86.36 cm, 100.44 cm, 126.37 cm, 152.40 cm, 182.80 cm, 197.50 cm, 287.02 cm. All coarse mesh boundaries are provided in Table I.

Other information necessary for use in PENMSH is the *upper bound* for the total number of fine cells along each axis available to further subdivide each coarse mesh. The PENMSH code defines material assignments/boundaries for each fine mesh. We defined the number of fine cells in each coarse mesh fundamentally based on the mean free-path of the x-rays in each material, along with memory requirements for the model. Medium mesh cell definitions are generated automatically by PENTRAN based on collapsing the fine mesh cell specifications for use with a spatial multi-grid acceleration.

All objects that are currently in X-ray Room #2 are explicitly modeled, except for the television monitor (used for viewing the fluoroscopic images output by the image intensifier), and a small lead film storage box in the wall, used to pass x-ray film into another room for developing. The TV monitor was omitted because it can be used in several locations in the room, making it difficult to model the room without considering an infinite number of configurations. The small lead box was omitted because it is in close proximity to the much larger personnel storage rack of lead jackets, and was determined have little impact on the model solution. A breakdown of the material constituents and properties, and the total number of mesh cells allocated to each is provided in Table II. The ability of PENTRAN to use discontinuous 3-D Cartesian cells was quite useful, given that nearly 86% of the problem volume was air, which has a very small attenuation of photons over the distances and energies considered in this problem. Also of note is the tissue phantom (modeled using a standard 4 element composition) had the highest average scattering ratio of all solid materials considered in the problem.

3.4 X-RAY SOURCE TREATMENT

Many x-ray studies are based on mono-energetic x-rays assumed to be at the maximum tube potential. In general, this is completely acceptable and conservative for general shielding design purposes. However, in our attempt to provide a more realistic assessment, we composed a multi-group model of the primary source beam. It is well known that an x-ray beam is a blend of both bremsstrahlung radiation (spanning a wide energy distribution) and characteristic x-rays (provided the tube potential is at a minimum of the characteristic peak edge). The resulting spectrum is based on the atomic number of the tube anode (in this case Z=74) with primarily K- and L-shell characteristic x-rays. Typically, L-shell characteristic x-rays are assumed to be completely attenuated within the x-ray tube housing (known as inherent filtration), whereupon x-rays below ~10 keV are cut off and assumed to be attenuated inside the source. Of course, this varies by tube manufacturer, although variations are often small. Approximately 10% to 15% of the spectrum is composed explicitly of K-a and K-b characteristic x-rays (59.32 keV, 67.24 keV, or 69.53 keV) for all source potentials above 70 kV. The remainder of the source (85% to 90%) comes from bremsstrahlung radiation in an energy continuum up to the tube potential cutoff.[11,12] To best represent the source, we used an 80 kV rotating tungsten anode x-ray source recently published in the literature by Bhat, et. al.[13] The reference spectrum was projected onto the appropriate photon groups of the BUGLE-96 broad group library.

Since the user can define multiple angular-energy-spatial dependent surface or volumetric sources anywhere in the problem geometry, the multi-group beam source was explicitly defined using a distribution of individual directions on the unit sphere. This was performed in PENTRAN using angular surface source specification cards. In this case, the source was placed as a collimated square of 693.9 cm^2 (approximately 10.5 by 10.5 inches square) surface area pointing downward into and centered on the patient tissue phantom (see Figure 2). Based on the predicted yields, the total time-integrated number of photons in the x-ray burst was 4.32E12.

3.5 GROUP DEPENDENT ALBEDO BOUNDARIES

PENTRAN allows for energy dependent albedo factors for each surface boundary. Therefore, energy dependent reflection albedos (e.g. J_g^-/J_g^+) were determined and used for the outer boundaries—the exterior lead and gypsum walls and the concrete floor—of X-ray Room #2. Since the ceiling was suspended, precise definition of components beyond it were not available, so the ceiling was treated as a vacuum boundary with zero return current. The availability of group-dependent albedo boundaries in PENTRAN allowed us to indirectly model scattering rather than require in-depth representations of the walls and floor in the large Room #2 model. Group albedo factors were determined using explicit, detailed PENTRAN *slab geometry* models of the walls and floor using an 80 kV x-ray source.

To accomplish slab albedo calculations in PENTRAN, reflective boundary conditions were defined for each boundary along *y*- and z- axes; along the *x*-axis, vacuum boundaries were used. Considering the large Room #2 model, we assumed all source photons were collimated and enter directly into the patient phantom *prior to interacting with any other material*. In doing so, we further assumed that x-ray interaction within the 100 cm of air between the x-ray source head and the surface of the patient phantom was negligible. Because source photons must initially pass through or scatter inside the patient phantom, the slab geometry models used to determine boundary albedos required that photons be first scattered through a tissue phantom before reaching boundary surfaces. Group dependent boundary albedo factors for the walls and floor determined for X-ray Room #2 using detailed slab geometry models are provided in Table III.

3.6 FLUX-TO-DOSE CONVERSIONS

The available photon response data for phantom related dose equivalents were interpolated and averaged from independent dose-response data.[11] Flux-to-dose conversion multipliers corresponding to the midpoint energies of each BUGLE-96 photon energy group (used to determine equivalent dose in Section 4) are provided in Table III. These group flux-to-dose conversion factors are listed in cSv-cm^2 soft tissue, equivalent to REM-cm^2 in soft tissue.

3.7 ADAPTIVE SPATIAL DIFFERENCING

A hybrid adaptive differencing method in PENTRAN was used throughout the problem in coarse mesh regions that contained solids. For each cell undergoing computation, this adaptive method selects either the DTW or EDW differencing scheme for each discrete direction; therefore, this scheme is completely adaptive for every direction in every cell in each energy group. The choice of scheme depends on the severity of the gradient of the computed angular flux. Initially, the DTW scheme is used; if DTW flux weights exceed 0.9, the EDW differencing scheme is used. For coarse mesh regions containing only air, the DTW scheme is specified, since there is little attenuation and therefore no need for an adaptive treatment in those areas.

4. RESULTS

Thus far, we have performed a single 3-D S_4 P_1 discrete ordinates calculation for the X-ray Room #2 model. Currently, additional studies with refinements of the space-angle mesh for this model are in progress, and will be made available in the near future. Discussions in this section are limited to the S_4 P_1 calculations. Convergence in all groups was obtained to an average relative tolerance of 0.5% throughout the model (verified by integral particle balance), with the exception of nine localized regions (not important to the calculation) that experienced 12% and smaller infinity norms. The nine regions included locations of severe attenuation, such as behind the lead jackets on the storage rack, and at the back of the electronics cabinets. Additional discretization is needed to improve the computational accuracy in those specific locations. Overall, the problem required 1 hour and 51 minutes to complete the four-group calculation using the 2-processor SPARKYcluster (discussed in Section 2.4) using angular decomposition in a multi-group source iteration sweep.

4.1 FLUENCE DATA

The graphical results we obtained for this problem are quite interesting. The plots presented in Figures 3a to 7b include density plots and surface plots of the resulting S_4 P_1 data for Groups 1 through 4 using a slice through the model at z=100 cm. Because PENTRAN allows the user to invoke 3-D discontinuous meshing among coarse mesh cells, the results were rendered from an 8-point 3-D weighted interpolation of group fluences. The values were rendered, starting from (5,5,100), proceeding at 10 cm intervals in both the x- and y-axis directions. Close inspection of the Group 1 data reveals evidence of slight ray effects, which are less pronounced in subsequent groups due to scattering. This is expected with S_4 quadrature, and should be less of an issue in future results with higher order angular quadratures and degrees of scattering order. If one studies the progression of plots from energy groups 1 to 4, one can clearly appreciate the penetration of the higher energies and subsequent absorption as the x-rays become colder. Of particular note is the severe attenuation of the flux by the lead jackets on the storage rack near x=100 cm. Also of interest is the leaded shield wall in the vicinity of the operator bunker. The right angle and long "trench" of the fluence caused by the this wall is clearly defined in each figure, as is the depression caused by the gypsum wall partition just beyond y=200 cm. Another interesting location is in the steel and glass storage cabinets, where there is no significant fluence depression until energy groups 4 and 5. The two high voltage electronics cabinets in the corner near x=400 cm are also interesting; the rear-most cabinet is taller than the other, and causes a jump in the fluence due to backscatter that is plainly visible. In each of the graphs, the interaction of the radiation with the support/imaging table is striking. Again, note that all radiation passes through the patient phantom first, which is then most likely scattered, and thereby continues on to interact throughout the table support material.

4.2 COMPARISON WITH EXPERIMENT

We compared our numerical dose calculations with experimental exposure measurement data. The experimental data was acquired for an 80 kV tube potential at 100.44 cm along the z-axis (centered on the surface of the support/imaging table). The measurement was collected

specifically for comparison with our total calculated dose. The peak soft tissue dose measured (converted from exposure units) at this point was 0.297 cSv, and the peak calculated soft tissue dose from the transport model was 0.294 cSv, for a relative difference of approximately 1%. Although this was the only data measurement available for comparison in this case, the excellent agreement for the total dose gave us confidence that our multi-group representation of the source in PENTRAN was correct with the s4 angular quadrature. For optimum problem resolution and minimization of some apparent ray effects, a higher order quadrature and scattering order representation are warranted; studies are ongoing to investigate this.

CONCLUSIONS

With the assumptions and broad-group structure used to model X-ray Room #2, it is encouraging that we obtained very close agreement with the experimental dose data near the source. Also, the solutions appear to be quite physical; the fluence density plots visually match the geometry of the room. Evidence of ray effects in the higher energies and limited resolution in isolated zones justify ongoing studies to further evaluate the space-angle discretization in this problem. Moreover, we plan to progress to studies involving fluoroscopic-mode steady-state x-ray sources. Long range, we believe this data will provide insight for operators to minimize radiation exposure, and permit better understanding of x-ray beam placement and facility design.

ACKNOWLEDGEMENTS

We gratefully acknowledge Dr Cynthia Elmore and SSgt J. Soriano of the 59th Medical Wing for providing us with the exposure data and valuable technical advice. Furthermore, we are grateful to Dr Ali Haghighat of the Pennsylvania State University and Dr John Garth of the Air Force Weapons Laboratory for their support and technical assistance.

REFERENCES

1. Sjoden, G., and A. Haghighat, "PENTRAN - A 3-D Cartesian Parallel Sn Code with Angular, Energy, and Spatial Decomposition," Proc for the Joint Int'l Conf on Mathematical Methods and Supercomputing for Nuclear Applications, Vol I, Saratoga Springs, New York, 1997.

2. Haghighat, A., H. Ait Abderrahim, and G. Sjoden, "Accuracy and Parallel Performance of PENTRAN Using the VENUS-3 Benchmark Experiment," ASTM STP 1398 on Reactor Dosimetry at the 10th International Symposium on Reactor Dosimetry, Osaka, Japan, 1999.

3. Haghighat, A., "PENINP.V3 for Automatic Problem Generation for PENTRAN," Penn State Transport Theory Group, The Pennsylvania State University, 1998a.

4. Haghighat, A., "PENMSH V.3 – A 3-D Cartesian Mesh Generator," Penn State Transport Theory Group, The Pennsylvania State University, 1998b.

5. Gropp, W., E. Lusk, and J. Skjellum, Using MPI: Portable Parallel Programming with the Message Passing Interface, MIT Press, Cambridge, Massachusetts (1994).

6. PENTRAN™, PENMSH™, PENINP™, PENPRL™ , 3DI™, and SPARKYcluster™, are trademarks of H&S Advanced Computing Technologies, Inc, of State College, PA, http://www.hsact.com.

7. VAST™ is a trademark of Pacific Sierra Research Corp, Santa Monica, CA, http://www.psrv.com.

8. Materials Handbook, 13th ed, McGraw Hill, Inc, New York.

9. Radiation Quantities and Units, Report 33, ICRU--International Commission on Radiation Units and Measures, Washington, D.C., 1980, p.20.

10. White, J., D. Ingersoll, C. Slater, and R. Roussin, "BUGLE-96: A Revised Multi-group Cross Section Library for LWR Applications Based on ENDF/B-VI Release 3", DLC-185, Oak Ridge National Laboratory, Oak Ridge, TN, 1996.

11. Chilton, A., and J. Shultis, and R. Faw, Principles of Radiation Shielding, Prentice-Hall Publishing, Englewood Cliffs, New Jersey (1984).

12. ICRU-17: "Radiation Dosimetry: X-Rays Generated at Potentials of 5 to 150 kV," ICRU Report 17, International Commission on Radiation Units and Measurements, Washington, D.C. 1970.

13. Bhat, M., J. Pattison, G. Bibbo, M. Caon, "Diagnostic X-ray Spectra: A Comparison of Spectra Generated by Different Computational Methods with a Measured Spectrum," Medical Physics, Vol 25(1), pp.114-120, January 1998.

TABLES

Table I: *x*-*y* and *z*-level Coarse Mesh Boundaries (units in cm)

	Bdy 1	Bdy 2	Bdy 3	Bdy 4	Bdy 5	Bdy 6	Bdy 7	Bdy 8	Bdy 9
x	0.00	111.76	248.92	374.0	439.43	575.95	--	--	--
y	0.00	58.42	149.86	361.95	549.19	--	--	--	--
z	0.00	60.16	86.36	100.44	126.37	152.40	182.80	197.50	287.02

Table II: X-ray Room #2 Preliminary Model; 131339 Total Cells

Material Name	Average Scatter Ratio*	Average Mfp cm*	Material Number	Fine Meshes	Volume cm^3	Percent Total Volume
Air	0.60	2938.	1	99496	7.79E+07	85.8
Pb+Air (Personnel Storage)	0.06	0.18	2	5025	7.39E+05	0.8
Stainless+Glass (Storage)	0.15	10.30	3	10433	2.14E+06	2.4
Tissue Phantom (4 element)	0.59	2.98	4	576	8.79E+04	0.1
Steel+Si (Electronics Cabinets)	0.20	1.18	5	11757	7.09E+06	7.8
Pb+Wall+Air (Primary Shield)	0.08	0.49	6	3232	2.21E+06	2.4
Wall+Air (Partition)	0.29	4.18	7	820	6.18E+05	0.7

*average for all energy groups

Table III: Group Source, Albedo, and Flux-to-dose Parameters

Model Group	BUGLE-96 Energy Group (number)	BUGLE-96 Upper Energy Bin (keV)	Source Fraction	Wall Albedo Factors	Floor Albedo Factors	Flux to Dose Factor (cSv- cm^2)
1	64	100	0.092	4.48E-05	7.82E-02	6.80E-11
2	65	60	0.596	5.24E-05	1.06E-01	4.96E-11
3	66	30	0.240	9.35E-04	6.69E-02	3.90E-11
4	67	20	0.072	3.55E-01	6.55E-00	3.50E-11

FIGURES

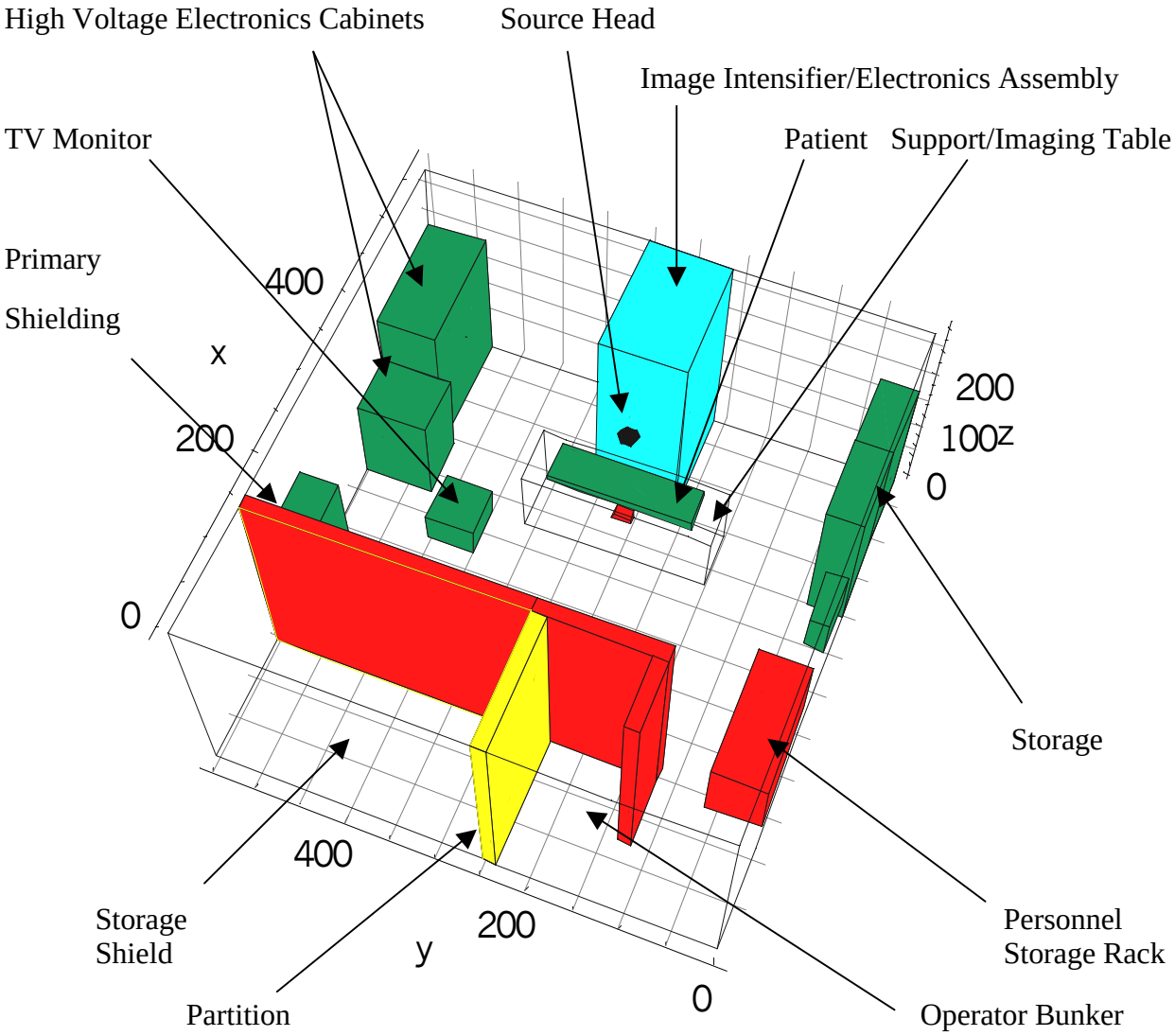

Figure 1: 3-D Schematic Model of X-ray Room #2.
(All dimensions are in cm; gridlines are equally spaced 50 cm apart).

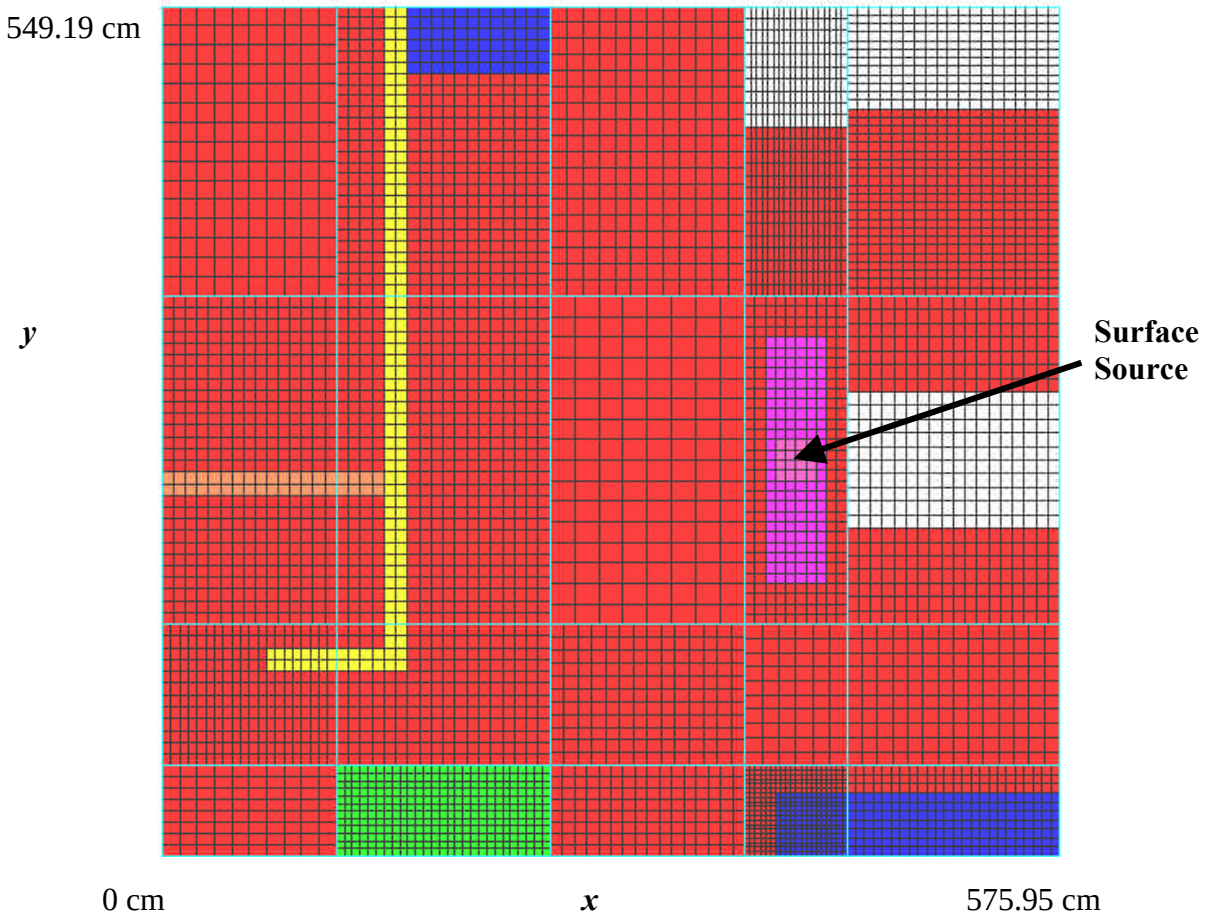

Figure 2. *z*-level 3: 86.6 cm to 100.44 cm along *z*-axis.

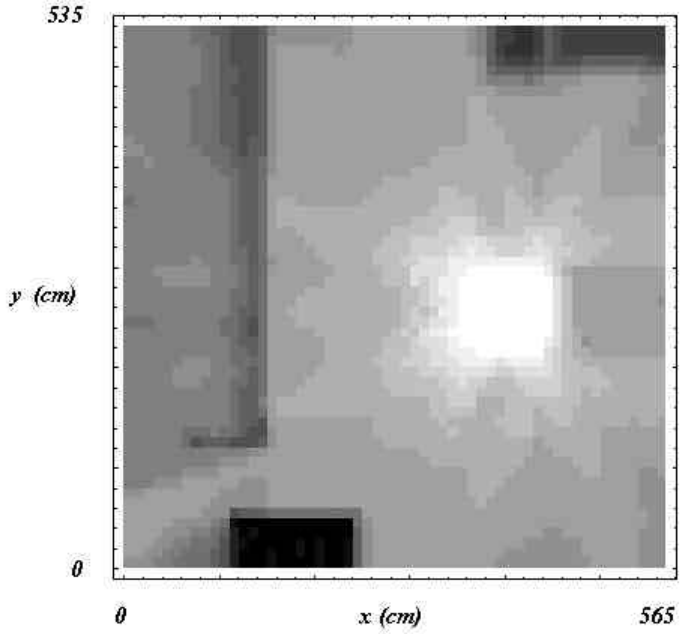

Figure 3a: Group 1 Fluence Density Plot, z=100 cm, S_4 P_1

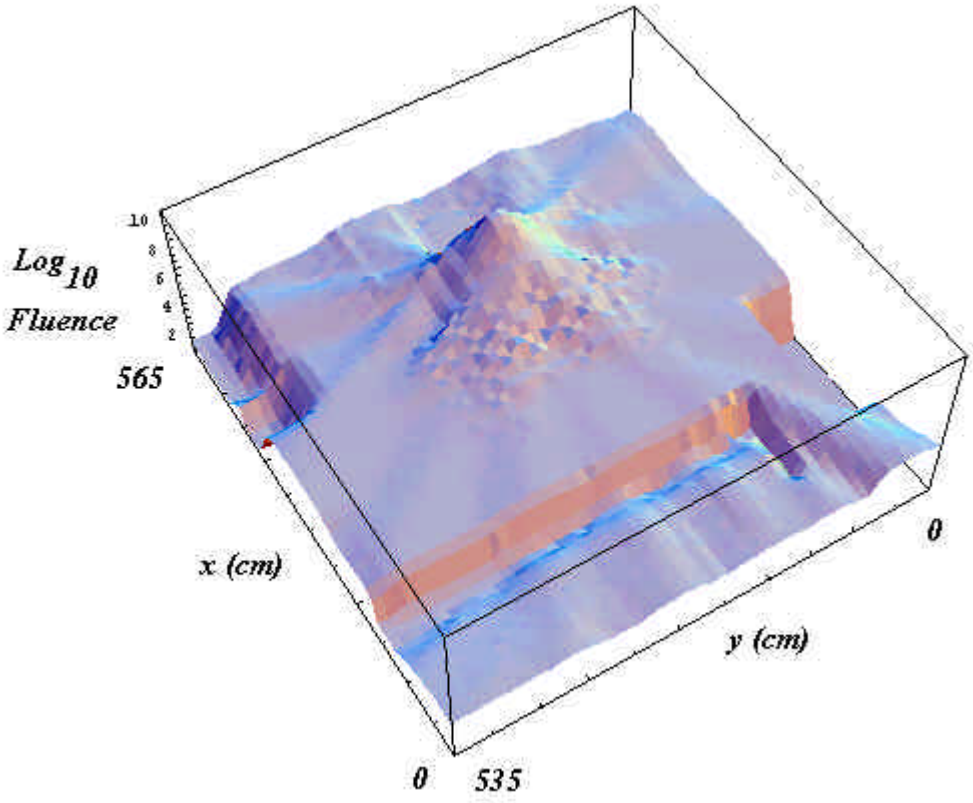

Figure 3b: Group 1 Log_{10} Fluence Surface Plot, z=100 cm, S_4 P_1

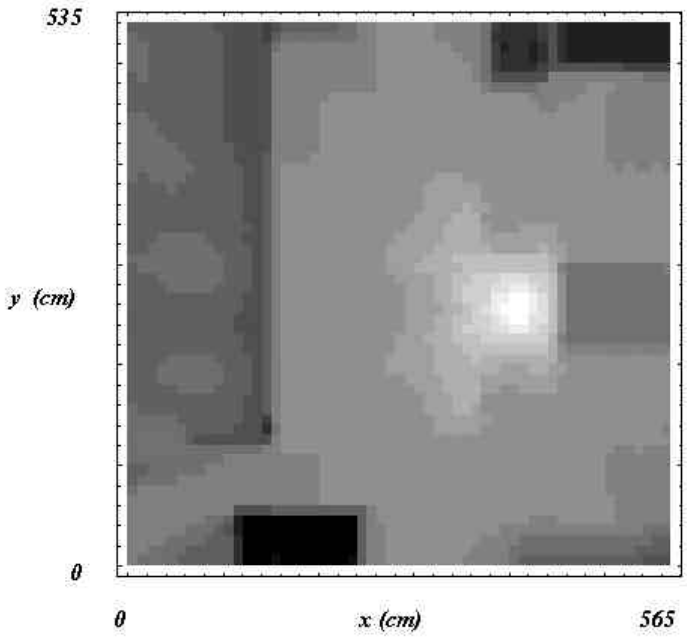

Figure 4a: Group 2 Fluence Density Plot, z=100 cm, S_4 P_1

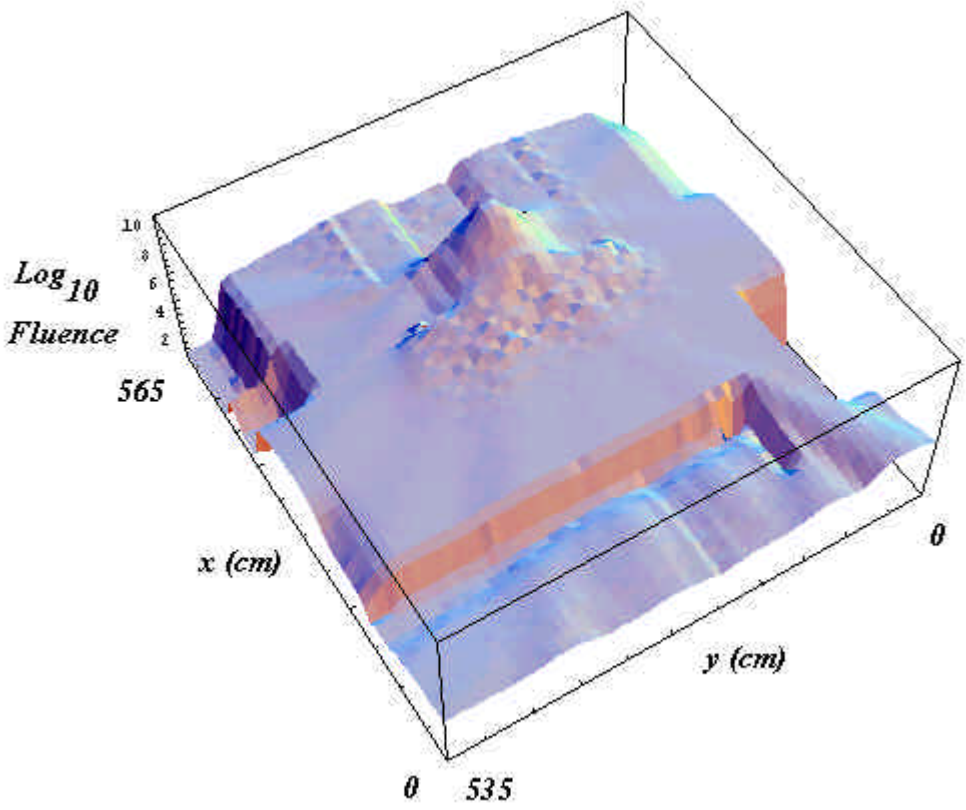

Figure 4b: Group 2 Log_{10} Fluence Surface Plot, z=100 cm, S_4 P_1

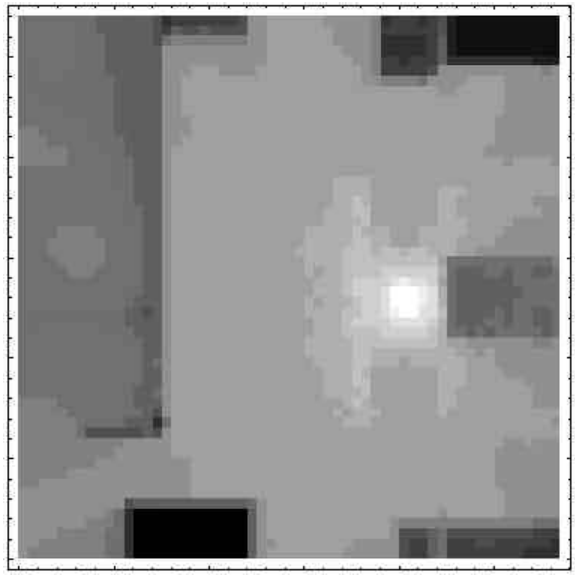

Figure 5a: Group 3 Fluence Density Plot, z=100 cm, S_4 P_1

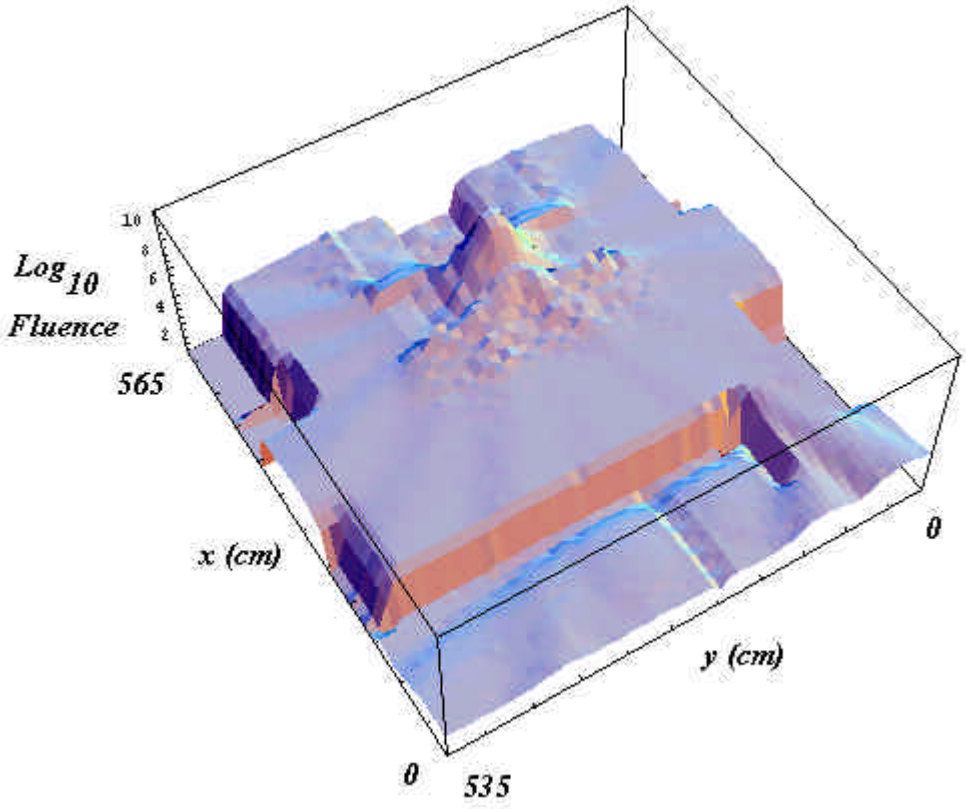

Figure 5b: Group 3 Log_{10} Fluence Surface Plot, z=100 cm, S_4 P_1

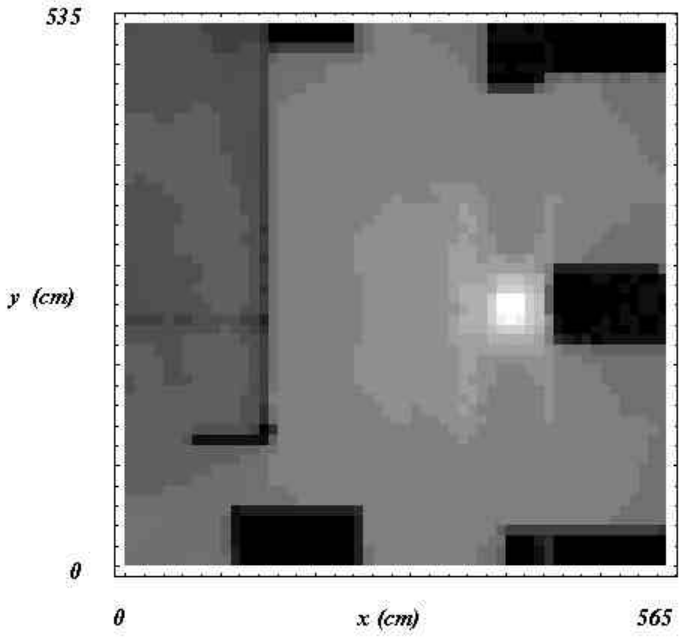

Figure 6a: Group 4 Fluence Density Plot, z=100 cm, S_4 P_1

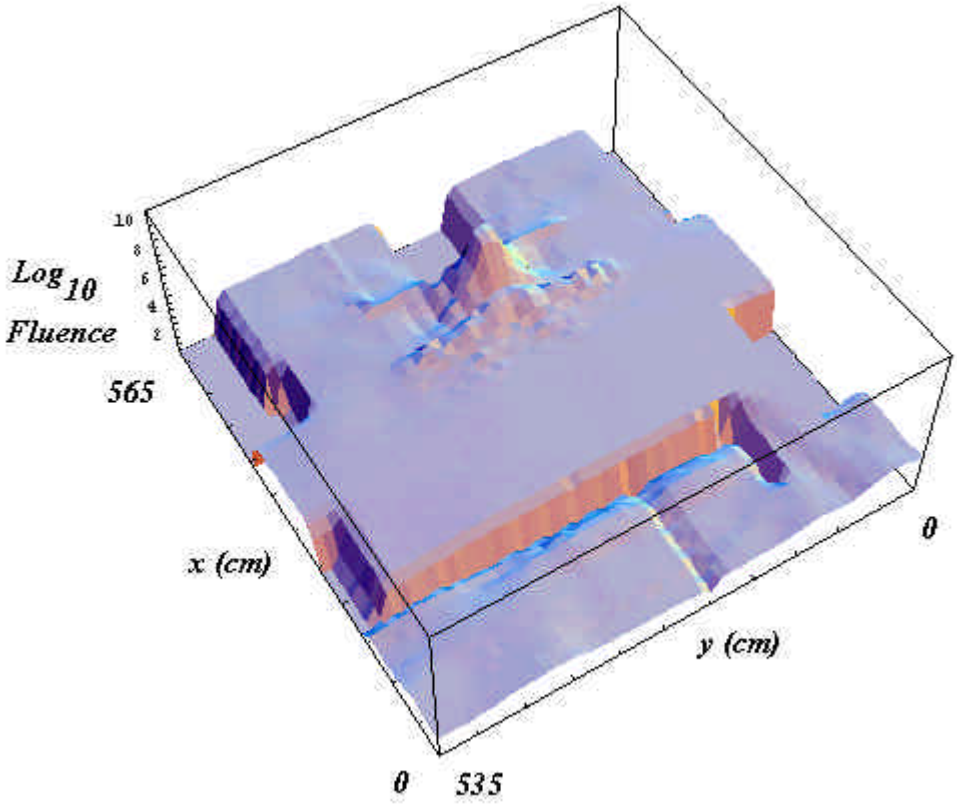

Figure 6b: Group 4 Log_{10} Fluence Surface Plot, z=100 cm, S_4 P_1

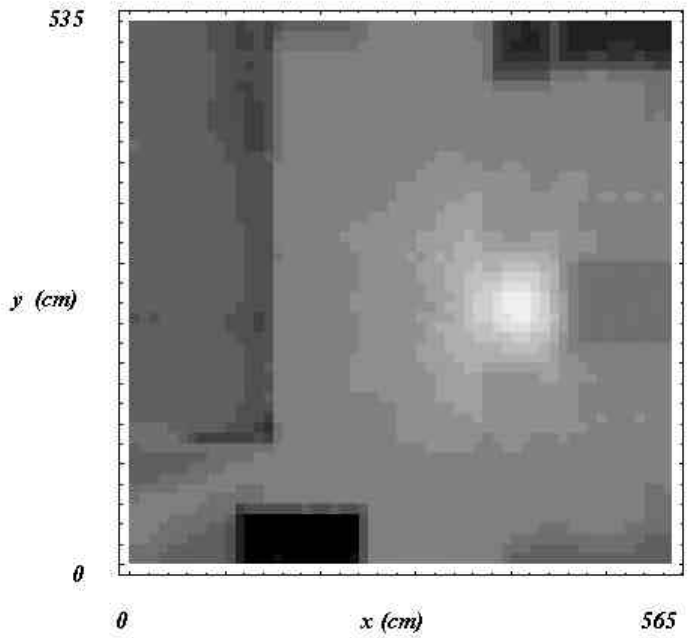

Figure 7a: Integral Dose (cSv Soft Tissue) Density Plot, z=100 cm, S_4 P_1

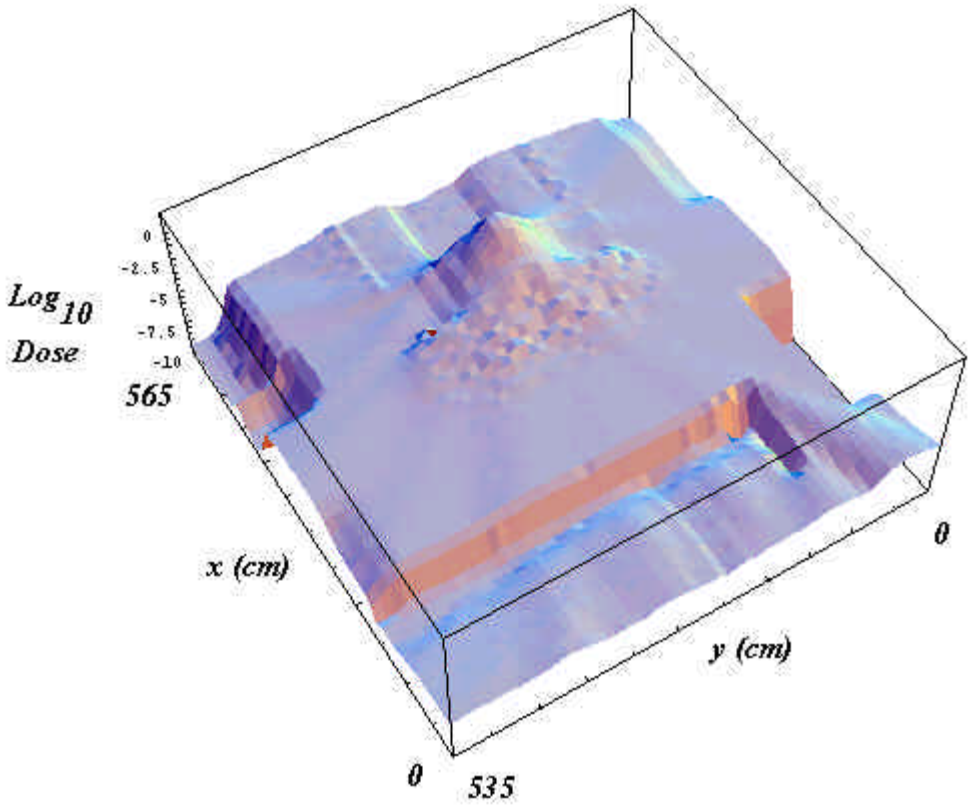

Figure 7b: Log Integral Dose (cSv Soft Tissue) Surface Plot, z=100 cm, S_4 P_1